Published in final edited form as:

ACS Nano. 2019 May 28; 13(5): 5493–5501. doi:10.1021/acsnano.9b00281.

Supramolecular Polymer Hydrogels for Drug-Induced Tissue Regeneration

Jing Cheng[†], **Devang Amin**[‡], **Jessica Latona**[§], **Ellen Heber-Katz**[§], **Phillip B. Messersmith**[*,†,‖]

[†]Departments of Bioengineering and Materials Science and Engineering, University of California, Berkeley, 210 Hearst Mining Building, Berkeley, California 94720, United States

[‡]Department of Biomedical Engineering, Northwestern University, Evanston, Illinois 60208, United States

[§]Laboratory of Regenerative Medicine, Lankenau Institute for Medical Research, Wynnewood, Pennsylvania 19096, United States

[‖]Materials Sciences Division, Lawrence Berkeley National Laboratory, Berkeley, California 94720, United States

Abstract

Supramolecular polymers self-assemble into nanofibers, micelles, and other nanostructures through weak noncovalent interactions between subunits. Such systems possess attractive properties for use in a variety of practical settings such as energy, sustainability, and healthcare. In regenerative medicine, a common approach involves implanting a supramolecular material containing cell and growth factor binding motifs directly into a diseased or traumatized tissue defect, whereupon it interacts with and/or recruits components of the biological system to induce tissue healing. Here we introduce a supramolecular therapeutic in which tissue regeneration is orchestrated by a supramolecular polymer prodrug implanted subcutaneously in a remote tissue. Our approach exploits a hydrophobic small-molecule inhibitor of prolyl hydroxylase enzyme as both a regeneration-inducing therapeutic and a structure-directing agent in a supramolecular polymer that forms shear-thinning nanofiber hydrogels. Subcutaneous injection of the supramolecular hydrogel in the back of mice wounded with a critical-sized defect in the ear led to transient upregulation of hypoxia inducible factor-1α and regeneration of ear tissue in a manner reminiscent of epimorphic regeneration. This drug-induced regeneration strategy utilizes a simple and translatable supramolecular design, eliminates the need for delivery of biologics (*e.g.*, growth factors, cells), and avoids implantation of a foreign material directly in a tissue defect.

[*]**Corresponding Author:** philm@berkeley.edu.

Author Contributions

J.C., E.H.K., and P.B.M. planned the experiments. J.C. performed all the *In vitro* experiments except cryo-EM. D.A. performed cryo-EM imaging. E.H.K. and J.L. performed the *in vivo* studies in mice and histological analysis of tissues. J.C., E.H.K., and P.B.M. wrote the manuscript.

The authors declare no competing financial interest.

Supporting Information

The Supporting Information is available free of charge on the ACS Publications website at DOI: 10.1021/acsnano.9b00281. Synthesis and characterization of DPCA and PEG–DPCA; cytotoxicity data; additional *in vivo* results; list of antibodies used in immunostaining (PDF)

Graphical Abstract

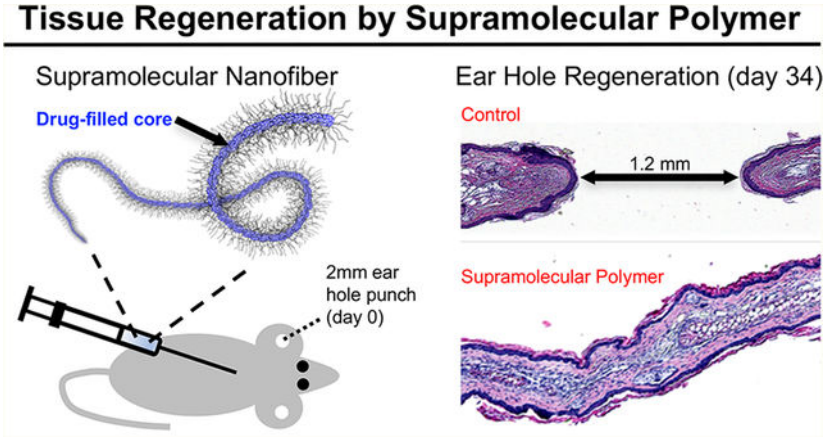

Keywords

supramolecular polymer; self-assembly; drug delivery; tissue regeneration; hypoxia-inducible factor

Supramolecular materials are composed of building blocks that assemble into higher order structures *via* weak noncovalent interactions.[1,2] These materials offer many attractive features for the design of materials through modular control of building block composition, order and disorder, and dynamic physical properties. One of the great opportunities for supramolecular materials lies in regenerative medicine, which is broadly concerned with the repair or regeneration of functional tissues as a treatment for traumatic injury, disease, or a genetic defect. Polymer hydrogels, including supramolecular polymers based on amphiphile, peptide, peptide–amphiphile, and ureidopyrimidinone self-assembly, have been extensively investigated for regenerative medicine and other medical applications.[3–5] Supramolecular polymers are often used in combination with biologic agents such as growth factors and cells that mediate local interactions with extracellular matrix molecules and host cells, leading to tissue regeneration. Supramolecular polymers with hydro-phobic domains for drug entrapment are well-suited for drug delivery and have been widely investigated as drug carriers for small-molecule chemotherapeutics, nucleic acids, and anti-inflammatory and antibacterial drugs.[6–8] However, supra-molecular systems that release small-molecule (nonbiologic) drugs that activate regenerative processes have not been described.

Drug-induced regeneration is an interesting alternative concept that has emerged in the past few years.[9,10] This approach employs small-molecule pharmacological agents to regenerate tissues through activation pro-regenerative host biological processes. In this report we describe the design of a supramolecular polymer prodrug for epimorphic tissue regeneration, a primitive regenerative process that relies on the plasticity of differentiated cells and local cues subsequent to wounding. Characteristic features of epimorphic regeneration include the formation of a blastema, cell dedifferentiation, and morphogenesis. Amphibians such as salamanders can regenerate entire limbs and other complex tissues through epimorphic regeneration, although mammals generally do not have this ability. One exception is found

in the Murphy Roths Large (MRL) mouse, an inbred strain that exhibits an unusual ability to regenerate tissues after wounding. MRL mice show traits of epimorphic regeneration, characterized by blastema formation, rapid epithelialization, cellular dedifferentiation, vascularization, and full regeneration. In the MRL mouse, critical size wounds of several tissues regenerate fully without scarring, including epidermis, dermis, cartilage, and hair follicles, whereas similar wounds in normal mice (*e.g.,* C57/BL6) form scars.[11–14] Recent research on adult MRL mice shows that a key feature of the MRL injury response is the maintenance of high levels of the transcription factor hypoxia inducible factor-1α (HIF-1α) in the first few weeks following injury.[9,15]

HIF-1α exerts its effects by transcriptional regulation of more than 100 gene products,[16,17] including those related to metabolism, angiogenesis, vasculogenesis, cell migration, and survival.[18] Prolyl-4-hydroxylase (PHD) regulates HIF-1α levels by hydroxylating proline residues, targeting the protein for processing and destruction by the ubiquitin–ligase complex.[19] Thus, PHD serves as a convenient control point for HIF-1α;[20,21] inhibition of PHD stabilizes HIF-1α. *In vitro* experiments showed that the PHD inhibitor 1,4-dihydrophenonthrolin-4-one-3-carboxylic acid (DPCA) is capable of stabilizing constitutive expression of HIF-1α protein.[9,22] Furthermore, tissue regeneration reminiscent of what is observed in MRL mice can be recapitulated in nonhealing mice through delivery of DPCA over a 10-day period *via* an injectable two-component polymer carrier.[9] In this study we used DPCA as both therapeutic and structure-directing building block of a supramolecular polymer system for tissue regeneration. Our aqueous supramolecular polymer hydrogel has shear-thinning properties to facilitate administration by simple injection and high drug loading and decomposes *in vivo* to produce only DPCA and poly(ethylene glycol) (PEG). The supramolecular polymer hydrogel induced *in vivo* ear hole regeneration in adult nonhealing mice, suggesting that supramolecular polymer hydrogels are attractive candidates for drug-induced tissue regeneration.

RESULTS/DISCUSSION

Self-Assembled Nanofibers of PEG-DPCA.

Initial studies of linear monomethoxy PEGs with a single terminal DPCA (P7D1 and P3D1) did not produce strong evidence of self-assembly in aqueous solutions (data not shown). To enhance the driving force for self-assembly and increase DPCA loading, three DPCA molecules were coupled *via* a trivalent linker to a 750 Da monomethoxy-PEG (P7D3). Transmission electron microscopy (TEM), cryo-TEM, and scanning electron microscopy (SEM) images of aqueous dispersions of P7D3 revealed the presence of nanofiber structures with an average fiber diameter of 5–8 nm and length of more than 1 μm (Figure 2a). The bundles of nanofibers observed by conventional TEM at higher concentrations (>3 mg/mL) and also in lyophilized P7D3 powder samples as shown in SEM images are likely to be due to drying effects. Small-angle X-ray scattering (SAXS) analysis of P7D3 revealed a −1 slope in the low-q range of the 1D scattering curve, confirming the presence of long cylinders (black curve in Figure 2b). The diameter of the cylinders was calculated to be 4.0 nm using a modified Guinier analysis (Figure S3), consistent with an order size of 4–6 nm for lyophilized P7D3 (red curve in Figure 2b) and 5–8 nm obtained from the TEM images.

Similar nanofiber morphologies have been reported for self-assemblies of amphiphilic PEG derivatives.[23,24] Thus, we consider the P7D3 nanofibers to be composed of a hydrophilic PEG corona and a hydrophobic core of DPCA, an arrangement that is consistent with the combined dimensions of the PEG chain (radius of the polymer in the mushroom regime $R_f \approx$ 1.85 nm)[25–27] and the DPCA molecule (~1.1 nm).

Supramolecular PEG-DPCA Hydrogels.

The continuous shear viscosity of aqueous P7D3 increased steeply at concentrations above 0.1 mg/mL (Figure S4), which was suggestive of entanglements formed by long nanofibers. Under oscillating shear, the storage modulus (G') of the nanofiber suspension was found to be low (10^2 Pa at 100 mg/mL) and only slightly higher than the loss modulus (G''), indicating liquid-like behavior. Recently, weak hydrophobic interactions were shown to enhance the stability of physically cross-linked hydrogels formed between derivatized biopolymers and polymeric core–shell nanoparticles.[28] On the basis of these principles, we synthesized a telechelic PEG–DPCA (P80D6) that was capable of gel stabilization by noncovalent bridging between nanofibers. Aqueous mixtures of P80D6 and P7D3 over a wide compositional range (17 different compositions at 100 mg/mL overall polymer concentration; see Table S1) were prepared by heating to 50 °C and cooling to room temperature. Qualitative visual observation indicated that gelation occurred within seconds upon cooling to room temperature for all compositions containing 25 mol % or more P7D3.

Detailed evaluations were performed for selected compositions using a combination of dynamic shear, frequency sweep, strain sweep, and step strain rheology (Figure 3). For brevity, we will focus on mixtures #3 and #12 (95:5 and 41:59 mol % P7D3:P80D6, respectively) as representative examples of low and high P80D6 content gels. Data on other compositions can be found in the Supporting Information (Figure S5). The frequency sweep of mixture #3 showed characteristics of viscoelastic hydrogels, with a loss modulus (G'') greater than the storage modulus (G') at low frequency and a crossover point above which $G' > G''$, indicative of more elastic-like behavior at high frequency (Figure 3a). Mixture #12 exhibited a crossover at substantially lower frequency than mixture #3, signifying higher gel stability at low frequency. Shear-thinning behavior is desirable in injectable hydrogels and often inherent in supramolecular hydrogels due to the dynamic nature of weak intermolecular interactions, which easily dissociate under applied shear stress and re-form when shear is removed.[28–32] Strain sweep curves of mixture #3 indicated that G' was largely strain independent except at very high strain ($\gamma > 100\%$); however mixture #12 exhibited a rapid decay in G' above 10% strain and ultimately behaved as a liquid ($G'' > G'$) above ~30% strain (Figure 3b). Step-strain measurements were performed in which a high instantaneous strain ($\gamma = 200\%$) was applied to break the network followed by constant low strain ($\gamma = 1\%$) to monitor the time-dependent recovery of the hydrogel. Hydrogel mixtures #3 and #12 exhibited a rapid decrease in G' followed by nearly complete recovery within seconds (Figure 3c), with no hysteresis in the recovery noted over several cycles.

The temperature-dependent rheological behaviors of mixtures #3 and #12 are shown in Figure 3d, and other compositions in Figure S6. A general trend of gradual decrease in G' with increasing temperature was observed in most cases, eventually reaching a crossover

point ($G' = G''$) that we defined as being a critical sol–gel temperature ($T_{sol–gel}$); mixtures behaved as liquids above and as gels below $T_{sol–gel}$. The values of $T_{sol–gel}$ for all compositions are listed in Table S1. Mixtures #3 and #12 were found to have $T_{sol–gel}$ values of ~42 and ~46 °C, respectively. Interestingly, mixture #3 remained highly viscous above $T_{sol–gel}$, whereas mixture #12 exhibited a more dramatic decrease in G' above the $T_{sol–gel}$ (G' decreased by 4 orders of magnitude from 20 to 50 °C). As this behavior was suggestive of differences in aggregation state above $T_{sol–gel}$, we performed SAXS of mixtures #3 and #12 at 37 and 50 °C (Figure S7). Indeed, we found that mixture #12 displayed a decrease in order at 50 °C compared to 37 °C, as indicated by attenuation of the peak at q values of 0.04–0.05 $Å^{-1}$, whereas order in mixture #3 remained nearly unchanged over the same temperature range.

Above 75 mol % P80D6 (mixtures #14–#17), mixtures had $T_{sol–gel}$ below 10 °C (data not shown) and behaved like liquids at room temperature (RT). The behavior in this regime is exemplified by pure P80D6, which at low concentration (>1 mg/mL, RT) formed micellar aggregates measuring 11 nm in diameter as determined by dynamic light scattering (DLS) (Figure S9). At higher concentrations (>25 mg/mL) micelles were bridged by telechelic P80D6 molecules, leading to a steep increase in viscosity (Figure S4). SAXS data confirmed this bridged micelle structure, where the −2.4 slope at low q (Figure S10, green line) indicated a cross-linked nanoparticle network[33,34] with order size ~12 nm, which matched the nanoparticle size determined by DLS. DLS (Figure S9) and SAXs data (Figure S10) showed that the bridged micelle structure of P80D6 disaggregated when heated to 50 °C, whereas P7D3 nanofibers were not affected by heating, suggesting that disruption of P80D6 bridges between nano-fibers occurs above $T_{sol–gel}$.

Summarizing all of the TEM, SAXS, DLS, and rheological data described above, several regimes of behavior were revealed, reflecting the supramolecular underpinnings of the P7D3/P80D6 system (Figure 4). Compositions within the red-shaded region in Figure 4a were stable gels at or below 40 °C and possessed a G' of at least 10^4 Pa, orders of magnitude greater than pure P7D3 and P80D6, which form nanofibers and micelles, respectively (Figure 4b left and right). P7D3/P80D6 mixtures within the range 5–65 mol % P80D6 likely consist of a basic framework of nanofibers of mostly P7D3 that are bridged by P80D6 (Figure 4b, middle). SAXS data on gels in this regime confirm the presence of cylindrical nanofiber structures, as evidenced by a slope of −1 in a modified Guinier plot (Figure S8). By virtue of its telechelic architecture P80D6 is capable of bridging nanofibers *via* hydrophobic interactions between DPCA end groups and the nanofiber cores, thus stabilizing the network. Due to the weak nature of the hydrophobic associations among DPCA end groups, shear stress or increased thermal energy can readily disrupt the network of nanofiber bridges and give rise to a gel–sol transition. Upon removal of shear, rapid reassociation of hydrophobic P80D6 end groups into the nanofiber cores occurs to re-establish a gel.

Our observations and interpretations are consistent with those of similar supramolecular telechelic and linear PEGs derivatized with self-associating end groups.[35–37] For example, Kieltyka *et al.* used SAXS, rheology, and EM to study ureidopyrimidinone (UPy)-derived PEGs to form supra-molecular hydrogel networks. These authors also mixed a low

molecular weight monofunctional PEG–UPy with telechelic UPy–PEG–UPy and obtained gel networks consisting of nanostructures bridged by the telechelic PEG chains.[37] Telechelic UPy–PEG–UPy systems have shown shear thinning and thermal melting behavior similar to what we have observed in our system.[35,36]

Drug Release, HIF-1α Upregulation, and Progenitor Cell Marker Expression *in Vitro*.

Ester linkages between PEG and DPCA afforded release of DPCA *via* hydrolysis. Preliminary *In vitro* experiments on pure P7D3 and P80D6 showed strong concentration-dependent DPCA release behavior (Figure S11a,b). For P7D3, DPCA release was very rapid at low concentration (>95% released within 1 day @ 1 μg/mL) but was considerably slower at high concentration (<5% release after 6 days @ 10 mg/mL). Similar trends were observed for pure P80D6, although at concentrations > 1 mg/mL release was approximately linear through the first 5 days. In view of the desirable shear-thinning and self-healing properties of gels #9, #10, and #12, we also performed *In vitro* drug release experiments of these mixtures (Figure S11c). An initial burst release of DPCA followed by an approximately linear release rate over a period of 12 days was observed for these gels, with DPCA release rate being generally slower in in gels with more P7D3. Gradual erosion of the hydrogel was observed, implying the disassembly of the gel by DPCA hydrolysis. Combining the results of drug release and rheological behavior, gels #10 and #12 were identified as the best candidates for further studies.

Cells isolated from regeneration-competent adult MRL mice are known to have higher expression levels of HIF-1α as well as a range of stem cell markers compared to cells from nonhealing B6 mice.[38] Following a favorable *In vitro* cytotoxicity study of gel #12 (Figure S12), we investigated whether we could induce an MRL-like phenotype in normal cells by exposure to supramolecular PEG–DPCA hydrogel. Ear-derived primary fibroblasts harvested from adult MRL and B6 mice were cultured in conditioned media[9] that had been exposed to gel #12 and then evaluated for cell marker expression (Figure 5). MRL fibroblasts (Figure 5, top row) stained positive for HIF-1α expression and a suite of progenitor cell markers, whereas untreated B6 fibroblasts (Figure 5, middle row) stained negative for these cell markers with the exception of slight positive staining of HIF-1α observed in dividing cells. In contrast, B6 fibroblasts treated with conditioned media for 24 h (Figure 5, bottom row) stained positive for HIF-1α expression as well as a number of progenitor cell markers, displaying similar patterns of cytoplasmic and nuclear staining found in primary MRL fibroblasts. B6 fibroblasts treated with PEG in the absence of DPCA stained negative for HIF-1α (data not shown), allowing us to attribute these results to release of DPCA from the supramolecular hydrogel as we had seen previously with the DPCA-trapped hydrogels.[9]

Supramolecular Hydrogel Induces Tissue Regeneration in Nonhealing Mice.

Swiss Webster mice were chosen to test the hydrogel therapy since they do not show a regenerative phenotype. We used an established ear hole punch model[11] that involves punching a 2.1 mm through-thickness hole in the ear and ascertaining tissue regeneration by physical measurements of ear hole closure combined with ear tissue harvesting and immunohistochemical analysis. A 25 μL amount of gels #10 and #12 and a PEG control

were administered by subcutaneous injection in the upper back at days 0 and 8. The host response at the injection site in the upper back 10 days after administration was minimal for the supramolecular hydrogel, revealing intact skin and underlying muscle with no evidence of the gel (Figure S13). In contrast, a tissue hematoma was observed in the PEG control group. Immunohistochemical staining of ear hole tissue revealed increased expression of HIF-1α from days 1 to 7 (Figure 6a) relative to mice without injection (data not shown). In the #10 hydrogel-treated mice, the ear holes closed to 0.5 mm on average after 34 days (Figure 6b), with a subset of ear holes closing completely (Figure 6c). In contrast, ear hole closure with the #12 gel was less effective (Figure S13). The control mice treated with PEG but no drug showed significantly less closure, culminating in an average ear hole size of 1.2 mm, which is characteristic of the typical response in nonhealing mice. Hematoxylin and eosin (H&E) and Alcian blue staining of control and gel #10 tissue sections harvested at day 34 showed clear evidence of new hair follicles and early cartilage formation (Figure 6d,e and Figure S14). Importantly, HIF-1α levels in #10 gel treated mice were found to return to normal (low) levels by day 13 (Figure S15), supporting the notion that we achieved a biphasic HIF-1α response similar to that seen in the MRL mouse during the regenerative response. Finally, we noted no adverse liver pathologies at days 20 and 27 for mice treated with #10 gel (Figure S16).

CONCLUSIONS

The molecular design of our supramolecular polymer prodrugs consists of hydrophobic DPCA end groups coupled to hydrophilic linear PEG polymers, exploiting DPCA as both structure-directing agent and therapeutic. Weak and reversible hydrophobic interactions between DPCA domains enable the hydrogels to flow under applied shear stress and to recover completely and immediately to the gel state when the stress is removed. These constructs have high drug loading and release DPCA by ester hydrolysis, leading to HIF-1α stabilization and tissue regeneration in otherwise nonhealing mice.

Our drug-induced regeneration approach utilizes many of the attractive features of supramolecular polymers such as compositional flexibility, modularity, dynamic physical properties, and biocompatibility. However, it departs in important ways from existing uses of supramolecular polymers for tissue regeneration, namely, the orchestration of tissue regeneration from afar. Furthermore, no sophisticated cell-interactive ligands, growth factors, cells, or other biologics are required. Finally, supramolecular polymer systems based on DPCA could be more broadly applicable in tissue regeneration, as MRL mice are capable of regeneration of a number of other tissues, including heart tissue and cartilage.[39,40]

METHODS/EXPERIMENTAL

Materials.

DPCA was synthesized as described.[9] All other reagents were purchased and used as received. Additional details are included in the Supporting Information.

Synthesis of P7D3 and P80D6.

P7D3 and P80D6 were synthesized from PEG and DPCA using CDI-activated esterification (details in the Supporting Information). The chemical structures of P7D3 and P80D6 were confirmed by NMR and LC-MS (Figure S2).

Preparation of P7D3 Nanofibers.

Polymer P7D3 was dissolved in DMSO to 20 mg/mL, added to 9 times the volume of water, and vortexed to form a viscous solution. The nanofibers were dialyzed in DI water for 2 days (4× water changes) and then lyophilized to a dry powder. The lyophilized powder was then dissolved in DI water or phosphate-buffered saline (PBS) buffer to a specified concentration.

Preparation of Hydrogels.

P7D3 and P80D6 solutions (100 mg/mL) were mixed with different ratios (see Table S1). The mixtures were warmed to 50 °C and mixed well by vortex for 5 min, then cooled to RT to get a homogeneous hydrogel.

Rheological Study.

Rheological characterization was performed on an oscillatory rheometer (MCR-302 modular compact rheometer by Anton Paar) with a parallel plate geometry (25 mm diameter, sand). Dynamic oscillatory strain amplitude, sweep, and step-strain behavior measurements were conducted at a frequency of 6.28 rad/s and 37 °C. Dynamic oscillatory frequency sweep measurements were conducted at 1% strain amplitude and 37 °C, 1% or 100% strain applied alternatively. Dynamic temperature-dependent sweep measurements were conducted at a frequency of 6.28 rad/s and 1% strain, with a 6 °C/min heating and cooling rate.

TEM and Cryo-EM.

P7D3 nanofiber solutions were dropped on carbon-coated copper grids for 2 min and stained for 1 min with 0.5% uranyl acetate aqueous solution for conventional TEM. TEM images were taken on a FEI Tecnai 12 transmission electron microscope. Samples for cryo-EM were prepared by vitrifying nanofiber solutions in liquid ethane using a Gatan Cryoplunge system. Cryo-EM imaging was taken on a JEOL 3200 TEM (Structural Biology Facility, Northwestern University).

In vitro Drug Release of Hydrogels.

A 50 μL amount of gel #12 was placed in a semipermeable membrane and suspended in 200 mL of PBS buffer (pH 7.4) in a capped glass vial. The vial was placed in a shaking incubator (100 rpm, 37 °C). The buffer was replaced with fresh PBS daily. For polymer solutions, 1 mL of P7D3 or P80D6 solution (from 1 to 100 mg/mL) was placed in 15 mL glass vials releasing DPCA in a shaking incubator (100 rpm, 37 °C). At designated time points an aliquot of buffer was removed and analyzed by HPLC with UV detection at 261 nm.

SAXS Study.

Small-angle X-ray scattering experiments were performed on Beamline 7.3.3 of the Advanced Light Source at Lawrence Berkeley National Laboratory. The polymer solutions

and hydrogels were loaded in 2.0 mm quartz capillaries and placed in a thermo-control device while acquiring data. The sample was probed at multiple locations in the capillary with a 10 keV synchrotron X-ray beam with a Mo/B4C double-multilayer monochromator. Samples were irradiated for 0.5 s. The 1D scattering profiles were obtained by radial integration of 2D patterns with scattering from PBS buffer in the capillary subtracted as background.

Cell Culture.

Primary ear dermal fibroblast cells were established from MRL and B6 mice.[9] Cells from early passages (<P20) were used in the described experiments. Cells were grown at 37 °C, 5% CO_2, and 21% O_2 in high-glucose Dulbecco's modified Eagle's medium (with L-glutamine) supplemented with 10% v/v fetal bovine serum, 20 mM HEPES, and 100 IU/mL penicillin/streptomycin.

Cytotoxicity Study.

B6 cells were grown overnight in 96-well cell culture plates. The cells were cultured for 24 h in media conditioned with gel extract as follows. Samples (10–40 μL) of gel #12, P7D3 (10 mg/mL), P80D6 (90 mg/mL), or PEG without DPCA (PEG750:-PEG8k = 1:9 w/w, 100 mg/mL) were added directly into wells containing cells and 100 μL of fresh media. Cell viability was measured by exposure to live–dead cell stain (ReadyProbes cell viability imaging kit by Life Technologies) for 15 min. Photomicro-graphs were produced using a fluorescent microscope (EVOS FL color imaging system), and the cell numbers were averaged from three different images.

Immunohistochemistry.

For immunohistochemical staining, MRL and B6 cells were seeded at 5000 cells per well in 96-well plates and grown overnight as described previously.[9] Cells were subsequently treated for 24 h with samples and controls as described above, then rinsed with PBS, fixed in cold methanol (−20 °C) for 10 min, rinsed with PBS, and treated with 10% goat serum and 0.1% Triton-X100 for 1 h. Then the cells were rinsed with PBS, incubated with the appropriate primary antibodies (diluted in 10% goat serum) at 5 °C overnight, rinsed with PBS, incubated with secondary antibodies (diluted in PBS) at RT for 1 h (in dark), and rinsed with PBS. Before imaging, 1 drop of antifade mountant with DAPI (Molecular Probes) was added to the wells and sealed with Greiner multiwell plate sealer (Sigma-Aldrich). Photomicrographs were taken using a fluorescent microscope (EVOS FL color imaging system).

In vivo Tissue Regeneration.

Ten-week-old female Swiss Webster mice were obtained from Charles River. On day 0, 2.1 mm ear hole punch wounds were created in ear pinnae, and then 25 μL of gel #10 or #12 was injected subcutaneously in the back of the neck.[9] The gel injection was repeated on day 8. At various time points, ear hole diameter was measured with calipers to monitor wound closure.

Tissue Histology.

As described elsewhere,[9] tissue from hole-punched ears and skin with underlying muscle taken from the injection site were fixed with Prefer fixative (the active ingredient is glyoxal) (Anatech) overnight and then washed in H_2O. Tissue was embedded in paraffin and cut into 5 μm thick sections. Tissue sections were dewaxed in xylene, rehydrated, and then stained with hematoxylin (Leica Microsystems, #3801562) and eosin (Leica Microsystems, #3801602) or Alcian blue. The stained slides were washed, rehydrated, cleared with xylene, and coverslipped with Permount mounting media (Fisher, SP15–500). Staining was visualized using an Olympus (AX70) microscope in bright field using a 4× objective and a Spot camera with bounded software.

Supplementary Material

Refer to Web version on PubMed Central for supplementary material.

ACKNOWLEDGMENTS

The authors acknowledge support from NIH grants R01 DE021104 and R01 DE021215. We also thank Dr. John Remis for help with cryo-EM at Northwestern University Structural Biology Facility, Khamilia Bedelbaeva for help with liver and ear tissue histology, and Dr. Chenhui Zhu for his help with SAXS experiments and data analysis. SAXS experiments were performed at Beamline 7.3.3 of the Advanced Light Source at Lawrence Berkeley National Laboratory. The Advanced Light Source is supported by the Director, Office of Science, Office of Basic Energy Sciences, of the U.S. Department of Energy under Contract No. DE-AC02–05CH11231. D.R.A. was supported in part by NIH grants T32GM008152 and T32GM008449.

REFERENCES

(1). Aida T; Meijer EW; Stupp SI Functional Supramolecular Polymers. Science 2012, 335, 813–817. [PubMed: 22344437]

(2). Liu K; Kang YT; Wang ZQ; Zhang X 25th Anniversary Article: Reversible and Adaptive Functional Supramolecular Materials: ″Noncovalent Interaction″ Matters. Adv. Mater 2013, 25, 5530–5548. [PubMed: 24038309]

(3). Boekhoven J; Stupp SI 25th Anniversary Article: Supra-molecular Materials for Regenerative Medicine. Adv. Mater 2014, 26, 1642–1659. [PubMed: 24496667]

(4). Goor OJGM; Hendrikse SIS; Dankers PYW; Meijer EW From Supramolecular Polymers to Multi-Component Biomaterials. Chem. Soc. Rev 2017, 46, 6621–6637. [PubMed: 28991958]

(5). Slaughter BV; Khurshid SS; Fisher OZ; Khademhosseini A; Peppas NA Hydrogels in Regenerative Medicine. Adv. Mater 2009, 21, 3307–3329. [PubMed: 20882499]

(6). Cheetham AG; Chakroun RW; Ma W; Cui H Self-Assembling Prodrugs. Chem. Soc. Rev 2017, 46, 6638–6663. [PubMed: 29019492]

(7). Vemula PK; Wiradharma N; Ankrum JA; Miranda OR; John G; Karp JM Prodrugs as Self-Assembled Hydrogels: A New Paradigm for Biomaterials. Curr. Opin. Biotechnol 2013, 24, 1174–1182. [PubMed: 23465753]

(8). Webber MJ; Langer R Drug Delivery by Supramolecular Design. Chem. Soc. Rev 2017, 46, 6600–6620. [PubMed: 28828455]

(9). Zhang Y; Strehin I; Bedelbaeva K; Gourevitch D; Clark L; Leferovich J; Messersmith PB; Heber-Katz E Drug-Induced Regeneration in Adult Mice. Sci. Transl. Med 2015, 7, 290ra92.

(10). Fan F; He Z; Kong LL; Chen Q; Yuan Q; Zhang S; Ye J; Liu H; Sun X; Geng J; Yuan L; Hong L; Xiao C; Zhang W; Sun X; Li Y; Wang P; Huang L; Wu X; Ji Z; et al. Pharmacological Targeting of Kinases Mst1 and Mst2 Augments Tissue Repair and Regeneration. Sci. Transl. Med 2016, 8, 352ra108.

(11). Clark LD; Clark RK; Heber-Katz E A New Murine Model for Mammalian Wound Repair and Regeneration. Clin. Immunol. Immunopathol 1998, 88, 35–45. [PubMed: 9683548]

(12). McBrearty BA; Clark LD; Zhang XM; Blankenhorn EP; Heber-Katze E Genetic Analysis of a Mammalian Wound-Healing Trait. Proc. Natl. Acad. Sci. U. S. A 1998, 95, 11792–11797. [PubMed: 9751744]

(13). Leferovich JM; Bedelbaeva K; Samulewicz S; Zhang XM; Zwas D; Lankford EB; Heber-Katz E Heart Regeneration in Adult Mrl Mice. Proc. Natl. Acad. Sci. U. S. A 2001, 98, 9830–9835. [PubMed: 11493713]

(14). Bedelbaeva K; Snyder A; Gourevitch D; Clark L; Zhang XM; Leferovich J; Cheverud JM; Lieberman P; Heber-Katz E Lack of P21 Expression Links Cell Cycle Control and Appendage Regeneration in Mice. Proc. Natl. Acad. Sci. U. S. A 2010, 107, 5845–5850. [PubMed: 20231440]

(15). Latona J; Shah A; Cheng J; Messersmith P; Heber-Katz E Enhanced Liver Regeneration after Partial Hepatectomy in Mice Treated with a Prolyl Hydroxylase Inhibitor. Am. J. Transplant 2017, 17, 462–462. [PubMed: 27343461]

(16). Semenza GL Hif-1 and Mechanisms of Hypoxia Sensing. Curr. Opin. Cell Biol 2001, 13, 167–171. [PubMed: 11248550]

(17). Banerji B; Conejo-Garcia A; McNeill LA; McDonough MA; Buck MRG; Hewitson KS; Oldham NJ; Schofield CJ The Inhibition of Factor Inhibiting Hypoxia-Inducible Factor (Fih) by [Small Beta]-Oxocarboxylic Acids. Chem. Commun 2005, 5438–5440.

(18). Liao D; Johnson RS Hypoxia: A Key Regulator of Angiogenesis in Cancer. Cancer Metastasis Rev 2007, 26, 281–290. [PubMed: 17603752]

(19). Bruick RK; McKnight SL A Conserved Family of Prolyl-4-Hydroxylases That Modify Hif. Science 2001, 294, 1337–1340. [PubMed: 11598268]

(20). Kim I; Mogford JE; Witschi C; Nafissi M; Mustoe TA Inhibition of Prolyl 4-Hydroxylase Reduces Scar Hypertrophy in a Rabbit Model of Cutaneous Scarring. Wound Repair Regen 2003, 11, 368–372. [PubMed: 12950641]

(21). Hill P; Shukla D; Tran MGB; Aragones J; Cook HT; Carmeliet P; Maxwell PH Inhibition of Hypoxia Inducible Factor Hydroxylases Protects against Renal Ischemia-Reperfusion Injury. J. Am. Soc. Nephrol 2008, 19, 39–46. [PubMed: 18178798]

(22). Love RJ; Jones KS Transient Inhibition of Connective Tissue Infiltration and Collagen Deposition into Porous Poly(Lactic-Co-Glycolic Acid) Discs. J. Biomed. Mater. Res., Part A 2013, 101, 3599–3606.

(23). del Barrio J; Oriol L; Sánchez C; Serrano JL; Di Cicco A; Keller P; Li M-H Self-Assembly of Linear–Dendritic Diblock Copolymers: From Nanofibers to Polymersomes. J. Am. Chem. Soc 2010, 132, 3762–3769. [PubMed: 20192188]

(24). Tan X; Li BB; Lu X; Jia F; Santori C; Menon P; Li H; Zhang B; Zhao JJ; Zhang K Light-Triggered, Self-Immolative Nucleic Acid-Drug Nanostructures. J. Am. Chem. Soc 2015, 137, 6112–6115. [PubMed: 25924099]

(25). Allen C; Dos Santos N; Gallagher R; Chiu GNC; Shu Y; Li WM; Johnstone SA; Janoff AS; Mayer LD; Webb MS; Bally MB Controlling the Physical Behavior and Biological Performance of Liposome Formulations through Use of Surface Grafted Poly(Ethylene Glycol). Biosci. Rep 2002, 22, 225–250. [PubMed: 12428902]

(26). Kienberger F; Pastushenko VP; Kada G; Gruber HJ; Riener C; Schindler H; Hinterdorfer P Static and Dynamical Properties of Single Poly(Ethylene Glycol) Molecules Investigated by Force Spectroscopy. Single Mol 2000, 1, 123–128.

(27). Lee H; Venable RM; MacKerell AD Jr.; Pastor RW Molecular Dynamics Studies of Polyethylene Oxide and Polyethylene Glycol: Hydrodynamic Radius and Shape Anisotropy. Biophys. J 2008, 95, 1590–1599. [PubMed: 18456821]

(28). Appel EA; Tibbitt MW; Webber MJ; Mattix BA; Veiseh O; Langer R Self-Assembled Hydrogels Utilizing Polymer–Nanoparticle Interactions. Nat. Commun 2015, 6, 6295–6303. [PubMed: 25695516]

(29). Guvendiren M; Lu HD; Burdick JA Shear-Thinning Hydrogels for Biomedical Applications. Soft Matter 2012, 8, 260–272.

(30). Yan C; Altunbas A; Yucel T; Nagarkar RP; Schneider JP; Pochan DJ Injectable Solid Hydrogel: Mechanism of Shear-Thinning and Immediate Recovery of Injectable [Small Beta]-Hairpin Peptide Hydrogels. Soft Matter 2010, 6, 5143–5156. [PubMed: 21566690]

(31). Bakota EL; Wang Y; Danesh FR; Hartgerink JD Injectable Multidomain Peptide Nanofiber Hydrogel as a Delivery Agent for Stem Cell Secretome. Biomacromolecules 2011, 12, 1651–1657. [PubMed: 21417437]

(32). Wong Po Foo CTS; Lee JS; Mulyasasmita W; Parisi-Amon A; Heilshorn SC Two-Component Protein-Engineered Physical Hydrogels for Cell Encapsulation. Proc. Natl. Acad. Sci. U. S.A 2009, 106, 22067–22072. [PubMed: 20007785]

(33). Schmidt PW Small-Angle Scattering Studies of Disordered, Porous and Fractal Systems. J. Appl. Crystallogr 1991, 24, 414–435.

(34). van Ommen JR; Valverde JM; Pfeffer R Fluidization of Nanopowders: A Review. J. Nanopart. Res 2012, 14, 737–765. [PubMed: 22593643]

(35). Bastings MMC; Koudstaal S; Kieltyka RE; Nakano Y; Pape ACH; Feyen DAM; van Slochteren FJ; Doevendans PA; Sluijter JPG; Meijer EW; Chamuleau SAJ; Dankers PYW A Fast Ph-Switchable and Self-Healing Supramolecular Hydrogel Carrier for Guided, Local Catheter Injection in the Infarcted Myocardium. Adv. Healthcare Mater 2014, 3, 70–78.

(36). Dankers PYW; Hermans TM; Baughman TW; Kamikawa Y; Kieltyka RE; Bastings MMC; Janssen HM; Sommerdijk NAJM; Larsen A; van Luyn MJA; Bosman AW; Popa ER; Fytas G; Meijer EW Hierarchical Formation of Supramolecular Transient Networks in Water: A Modular Injectable Delivery System. Adv. Mater 2012, 24, 2703–2709. [PubMed: 22528786]

(37). Kieltyka RE; Pape ACH; Albertazzi L; Nakano Y; Bastings MMC; Voets IK; Dankers PYW; Meijer EW Mesoscale Modulation of Supramolecular Ureidopyrimidinone-Based Poly(Ethylene Glycol) Transient Networks in Water. J. Am. Chem. Soc 2013, 135, 11159–11164. [PubMed: 23829684]

(38). Naviaux RK; Le TP; Bedelbaeva K; Leferovich J; Gourevitch D; Sachadyn P; Zhang X-M; Clark L; Heber-Katz E Retained Features of Embryonic Metabolism in the Adult Mrl Mouse. Mol. Genet. Metab 2009, 96, 133–144. [PubMed: 19131261]

(39). Leferovich JM; Bedelbaeva K; Samulewicz S; Zhang X-M; Zwas D; Lankford EB; Heber-Katz E Heart Regeneration in Adult Mrl Mice. Proc. Natl. Acad. Sci. U. S. A 2001, 98, 9830–9835. [PubMed: 11493713]

(40). Chu CR; Szczodry M; Bruno S Animal Models for Cartilage Regeneration and Repair. Tissue Eng., Part B 2010, 16, 105–115.

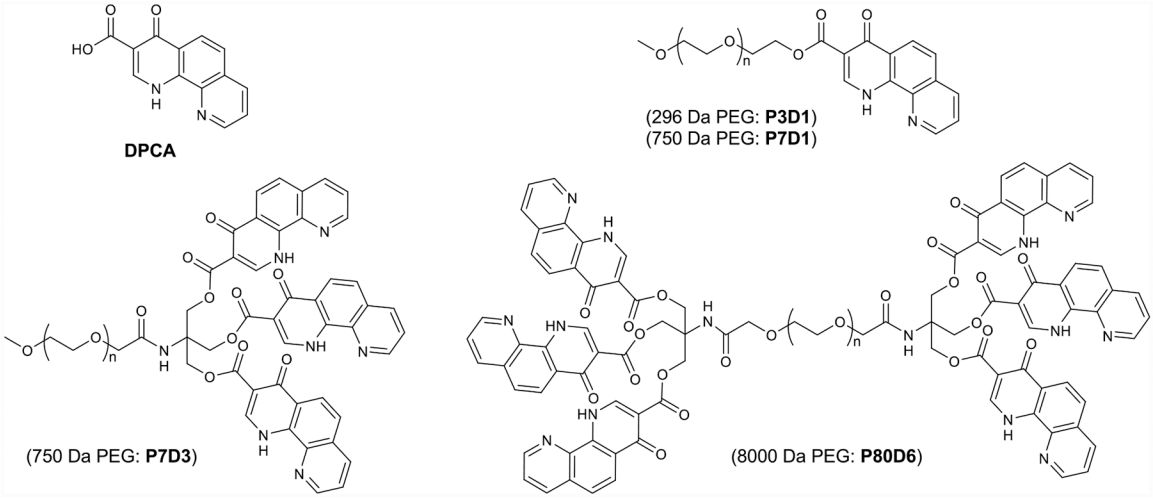

Figure 1.
Chemical structures of DPCA and PEG–DPCA conjugates studied.

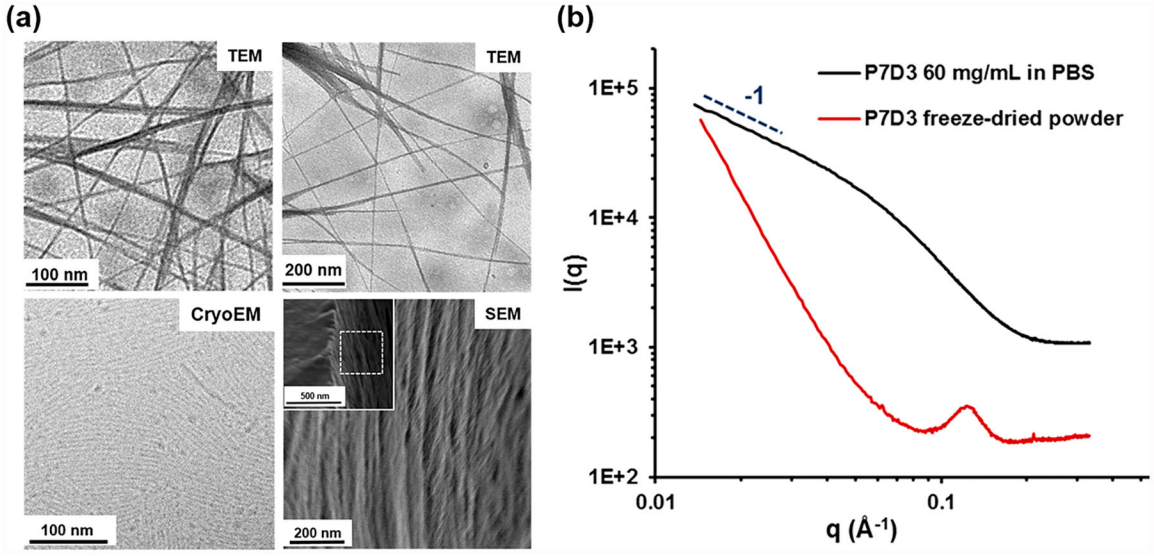

Figure 2.

P7D3 forms nanofiber assemblies. (a) EM images of P7D3 nanofibers obtained by TEM (3 mg/mL), cryo-TEM (1 mg/mL), and SEM (lyophilized powder). (b) SAXS patterns show a cylindrical form factor, as indicated by the −1 slope at low *q* of the aqueous sample, and a scattering peak of the powder sample suggesting a feature size of 5–8 nm.

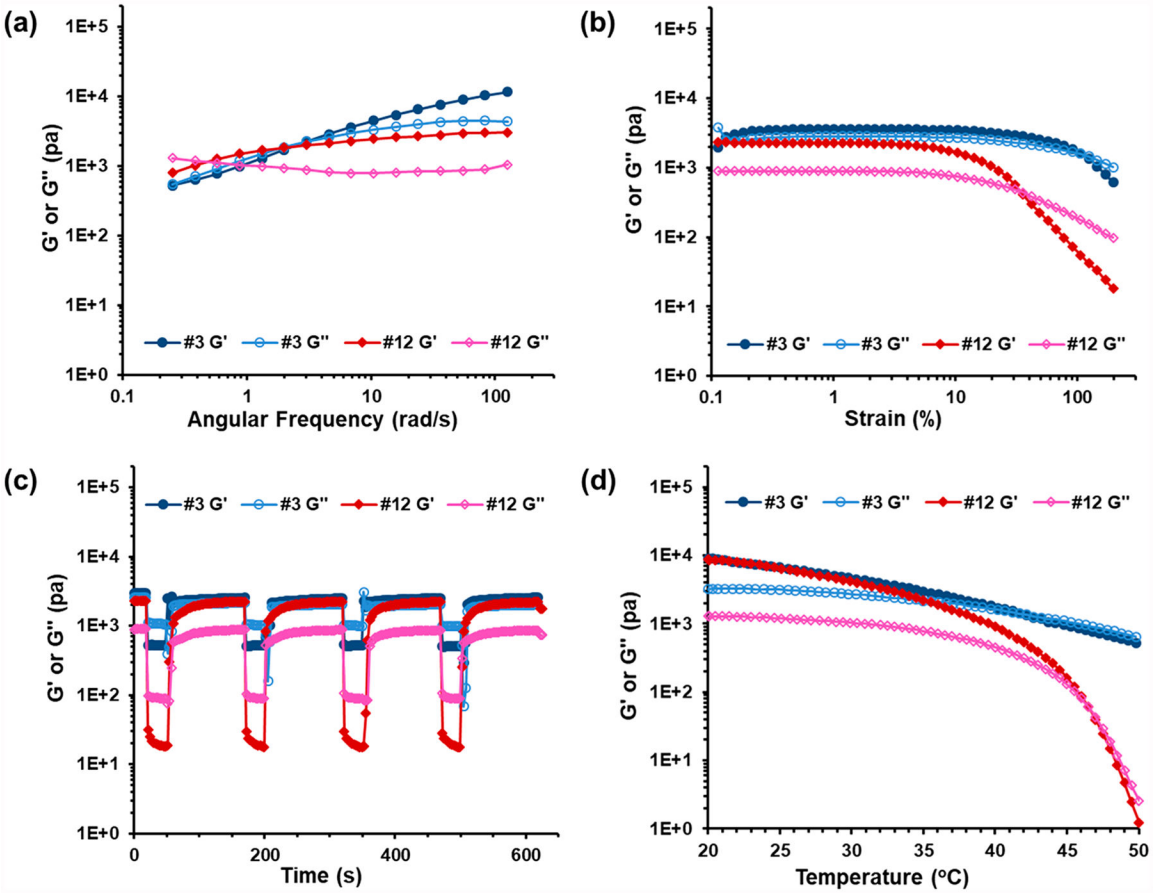

Figure 3.

Rheological behavior of self-assembled P7D3/P80D6 hydrogels #3 and #12. (a) Frequency sweep at $\gamma = 1\%$, 37 °C; (b) strain sweep at $\omega = 6.28$ rad/s and 37 °C; (c) step-strain behavior $\gamma = 1\%$ or $\gamma = 200\%$, $\omega = 6.28$ rad/s, 37 °C; (d) temperature sweep, $\gamma = 1\%$, $\omega = 6.28$ rad/s, heating rate 6 °C/min.

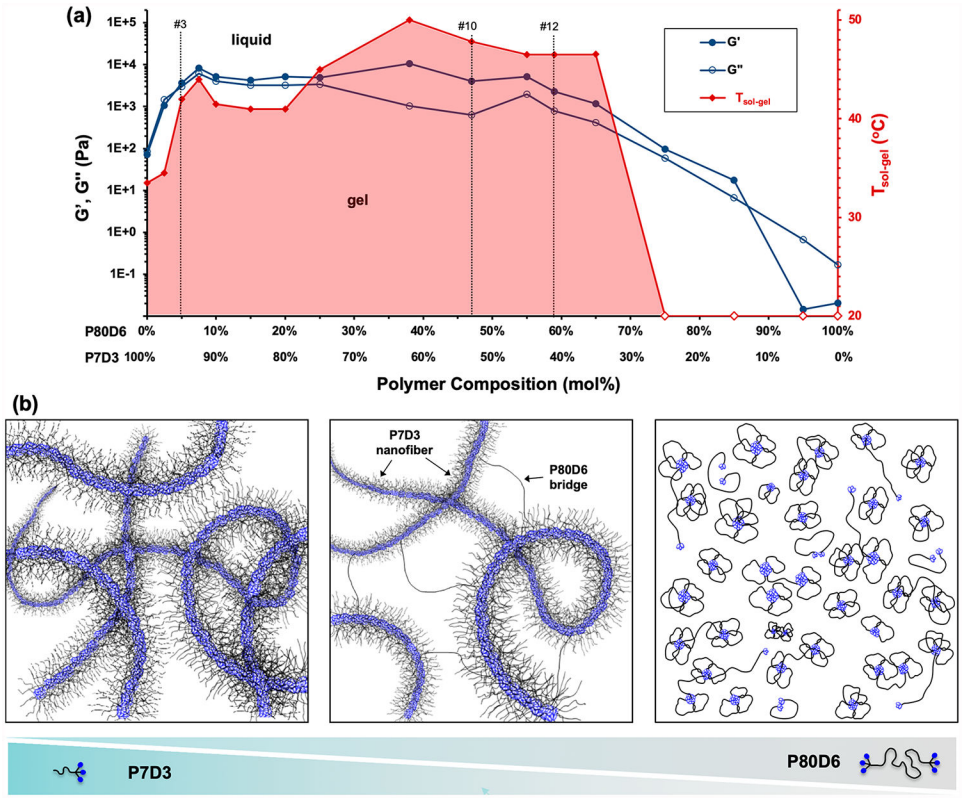

Figure 4.

Summary of thermorheological and self-assembly behavior of supramolecular PEG–DPCA hydrogels. (a) Effect of composition on rheological and thermal sol–gel transition temperature ($T_{sol–gel}$). The left *y*-axis shows G' and G'' obtained at $\omega = 6.28$ rad/s, $\gamma = 1\%$, $T = 37$ °C. The right *y*-axis shows $T_{sol–gel}$, identified in temperature sweep experiments ($\omega = 6.28$ rad/s, $\gamma = 1\%$) as being the temperature at which $G' = G''$. Mixtures behaved as liquids at temperatures above $T_{sol–gel}$ and as gels below $T_{sol–gel}$. The red unfilled diamonds indicate that no gelation was observed above 10 °C. The vertical dashed lines indicate the compositions of gels #3 and #12. All analyses were performed at 100 mg/mL. (b) Schematic illustration of supramolecular assemblies of PEG–DPCA. Self-assembly of P7D3 and P80D6 is driven by hydrophobic interactions among DPCA end groups, forming nanostructures with DPCA-rich cores (blue) and PEG corona (black). Shown on the left is a representation of nanofibers formed by pure P7D3, whereas on the right is a representation of micelles formed at high concentration of pure P80D6. The schematic shown in the middle depicts the proposed structure for the #10 or #12 gels that contain a mixture of P7D3 and P80D6. In this case, the structure consists of primarily P7D3 nanofibers that are bridged by P80D6.

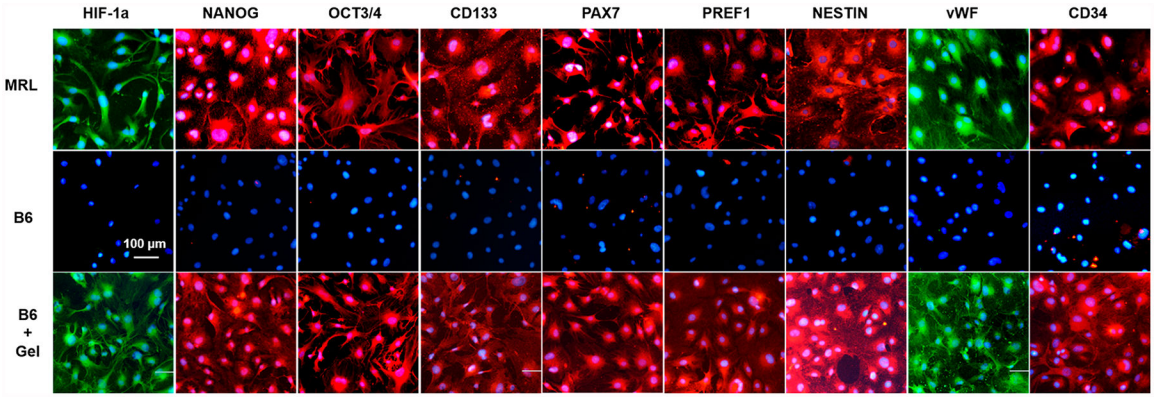

Figure 5.

Release of DPCA from supramolecular hydrogel upregulates HIF1α and induces a progenitor cell phenotype. HIF-1α stabilization and progenitor cell marker expression induced by supramolecular hydrogels. MRL mouse fibroblasts (top row), B6 mouse fibroblasts (middle row), and B6 mouse fibroblasts cultured with extract from hydrogel #12 (bottom row) were grown for 24 h in 96-well plates and immunostained with antibodies against HIF-1α, NANOG, OCT3/4, CD133, PAX7, PREF1, Nestin, von Willebrand factor (vWF), and CD34.

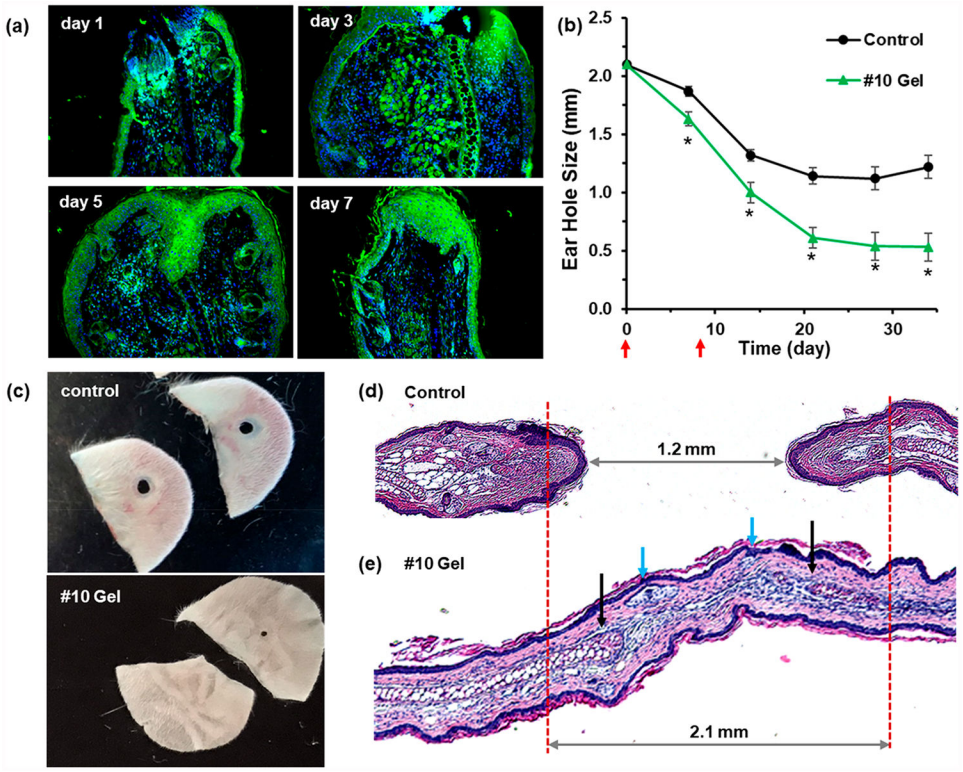

Figure 6.

Supramolecular hydrogels enhance tissue regeneration in Swiss Webster mice. Swiss Webster mice were injected subcutaneously with 25 μL of gel #10 or PEG (control) on days 0 and 8 after ear hole punching. (a) Ear tissue was harvested on day 1, 3, 5, or 7 for HIF-1α immunostaining (green). (b) Ear hole closure *versus* time for control and #10 gel treated group. The red arrows indicate time points at which supramolecular gel was administered (n = 10 ears, $p < 0.005$ *vs* control for all time points). (c) Example photographs of ear holes taken on day 35 for control group and day 34 for #10 gel treated group. (d, e) Histological tissue sections of H&E-stained ear tissue taken on day 34 from control mice (d) and #10 gel treated mice (e). The blue arrows indicate the new hair follicles, and the black arrows indicate the early cartilage formation. Images with higher resolution and Alcian blue staining are shown in Figure S14.